ALMA Memo 523

Simulation of Atmospheric Phase Correction Combined With Instrumental Phase Calibration Using Fast Switching

Originally LAMA Memo 803 2004 Jan 239

M. A. Holdaway and L. D'Addario
National Radio Astronomy Observatory
949 N. Cherry Ave, Tucson AZ 85721-0655
contact author: mholdawa@nrao.edu

LAMA Memo 803
Simulation of Atmospheric Phase Correction Combined With Instrumental Phase Calibration Using Fast Switching

M.A. Holdaway and L. D'Addario
National Radio Astronomy Observatory
949 N. Cherry Ave.
Tucson, AZ 85721-0655
email: mholdawa@nrao.edu

January 23, 2004

Abstract

We present very detailed simulations of fast switching phase correction which treats, as accurately as we can, fast switching at all frequency bands available to ALMA, with the calibration being performed at either the target frequency or at 90 GHz.

This work leads us to the following results and potential problems:

- Fast switching will typically have efficiencies (considering both residual decorrelation and time spent calibrating) ranging from 0.70 at the highest frequencies to 0.90 at the lowest.
- Residual phase errors will range from 35 deg rms at the highest frequencies to 15 deg rms at the lowest frequencies.
- For target frequencies above 345 GHz, calibrating at 90 GHz (where the sources are brighter and the sensitivity is better, but requires an extra calibration observation to determine the difference in the instrumental phases at the two frequencies) will result in about a 5% increase in efficiency over calibrating at the target frequency. It appears that below 345 GHz, there is little gain in performing the calibration at 90 GHz, and we may very well calibrate at the target frequency.
- Performing fast switching at 90 GHz, rather than at the target frequency, only improves the efficiency by about 5% in the sub-millimeter, and may be deemed too much trouble for too little gain.
- Problems with modeling dispersive delay in the sub-millimeter regime, or dry path-length fluctuations together with even well-modeled dispersive delay, could push us to perform calibrator observations at the target frequency above 345 GHz.
- Calibrator sources (ie, flat spectrum quasars) might not look the same at 90 GHz and the target frequencies because of dust emission at the higher frequency, or because the position of the core changes with frequency. These effects could make it difficult to calibrate at a frequency other than the target frequency.
- The fast switching pointing specification (being able to move 1.5 deg in 1.5 sec with a 3 arcsec residual pointing error) is not acceptable for mosaicing or sub-millimeter

observations, and we need to study how quickly the antenna returns to an acceptable pointing residual.

- The specification on changing frequencies is 1.5 s, which was intended to match the fast switching antenna motion specification. If this could be shaved to 1 s, we could probably make good use of that improved frequency change time.
- At the best 5% conditions in the joint opacity/phase stability distributions, we determine that the residual phase jitter over short times (ie, 20 s or less) is 111 fs rms delay.
- Also at the best 5% atmospheric conditions, simulations indicate that longer timescale (ie, 300 s) atmosphereic delay variation will produce residual errors in visibility phase corresponding to about 32 fsec rms.

1 Introduction

1.1 Phase Errors are Really Bad

Phase fluctuations due to the atmosphere are really bad. If unchecked, they will result in:

- decorrelation, which means a loss of sensitivity.
- the decorrelation will actually be variable, leading to visibility amplitude fluctuations. These in turn will complicate the flux calibration and limit the image quality.
- phase errors, which basically limit our ability to determine where anything really is, messing up our images and limiting our resolution.

Chajnantor may be one of the best millimeter and sub-millimeter sites in the world, but let me let you in on a little secret: for the median phase stability conditions measured by Simon Radford's 300 m baseline interferometer, if we were to leave the phase fluctuations uncorrected at 230 GHz on that same 300 m baseline, the coherence would only be 0.5! That's more than half of ALMA's sensitivity down the drain for half of the time, at the relatively low frequency of 230 GHz and relatively short baselines of 300 m. Remember this: Chajnantor is an excellent site as judged by transparency, but when you look at the phase stability, ALMA is only marginally better than other sites (for example, our ALMA site has about 25% better phase stability than our measurements from the VLBA site on Mauna Kea).

Yes, phase errors are really bad.

The statistical nature of the phase fluctuations above Chajnantor is well understood – every ten minutes, we determine the phase structure function from the site testing interferometer data, which permits us to calculate the phase errors on any desired time or spatial scale, at any observing frequency. We have trouble extrapolating far beyond the 300 m baseline which the site testing interferometer measures, as the phase structure function is expected to flatten somewhere around 500 or 1000 m – depending upon the thickness of the turbulent atmospheric layer. However, as we can see, if you are worried about what the phase structure function is doing at 1000 m, you've already lost the war. All the action is down on short time and spatial scales.

1.2 But Phase Errors Can be Corrected

Of course, we've been worrying intensely about the problem of phase correction on ALMA for over a decade, and it is widely appreciated that we must win the battle for phases at the shortest possible time scales. The two competing correction methods are **water vapor radiometry** (aka WVR; Hills and Gibson, 2001; Delgado 2001, Delgado *et al*, 2003), which will perform well on time scales as short as 1 s, but has problems tying in the fluctuations to absolute water vapor levels (ie, has trouble with the long scales) – and **fast switching**, which, with typical switching time scales of 20 seconds, will effectively remove atmospheric structure on time scales of about 10 seconds, and has no problems hooking into longer time scales. WVR's problems on long time scales are due, not only to long time scale instrumental stability, but also because WVR does not directly measure the water vapor, but must infer it from brightness temperature measurements via an inexact model; furthermore, the delay must be inferred, via a model, from the inferred water vapor.

The BIG hope is that these two seemingly complimentary phase compensation methods might work together as a coherent phase compensation strategy, but constructing and verifying such a strategy requires either extensive simulations beyond our current capabilities, or an operating ALMA with which to experiment. If we cannot use WVR to improve the short time scale fluctuations which fast switching cannot touch, we will need to deal with extensive correction for decorrelation, which will be both baseline and time dependent (Holdaway, 2003b, unpublished).

2 Overview of Fast Switching

2.1 Fast Switching with Calibration at the Target Frequency

Fast switching phase correction is a phase compensation strategy which solves for the antenna-based phases – which will be a combination of the atmospheric and instrumental phases – by quickly observing a moderately bright point source calibrator and quickly rushing back to the target source to observe for a limited integration. However, as the atmosphere changes and the calibrator phase solutions go stale, we must go back and observe the calibrator again. With the nearly complete record of atmospheric phase stability data from Simon Radford's site testing campaign at Chajnantor, and our detailed understanding of the fast switching phase correction process, we can calculate fairly precisely how often we must observe that calibrator and how much sensitivity we will lose by calibrating instead of observing, and how much sensitivity will be lost due to decorrelation from the imperfectly calibrated phases. While there are many populations of sources which could serve as phase calibration sources, we think that the quasars will provide a good combination of being both ubiquitous and unresolved.

Fast switching has been shown to work at several millimeter observatories. It is generally accessible to all telescopes, as it is little more than traditional phase and amplitude calibration, only done on time scales short enough to actually track some or most of the atmospheric fluctuations. However, as no telescope before ALMA has been designed with fast switching in mind, on existing telescopes, we take what the telescope provides in terms of calibration strategies. On ALMA, we expect to see a highly tuned version of fast switching achieve the most we can, given what nature provides us in terms of the atmospheric conditions and the sky full of calibration sources.

As a prelude to the next section, remember that fast switching at the target frequency measures the sum of the instrumental and the atmospheric delays with every calibrator observation and requires nothing special.

2.2 Fast Switching Observing the Calibrator at a Lower Frequency

But ALMA will go yet another step beyond what existing telescopes are able to do: it is planned that ALMA will perform the phase calibration at the relatively low and sensitive frequency of 90 GHz and scale the phases, presumed due to non-dispersive atmospheric delays (we treat dispersive delays later), up to the observing frequency. We'll refer to this as dual-frequency fast switching. Our past calculations of ALMA's fast switching efficiency have appreciated the fact that the phase solutions at the lower frequency have to be very accurate in order to scale them to the target frequency. While we knew we would need to periodically observe a bright calibrator at both the calibrator and target frequencies to solve for the instrumental phases at both frequencies, we have never calculated the impact this so-called instrumental sequence (also referred to as the cross-band calibration in some documents) would have on fast switching efficiency. We needed an estimate of the brightness of the calibration sources as a function of frequency, and it wasn't until now that we have developed such estimates. In order to more accurately predict the efficiency of fast switching phase correction on ALMA, we also need to make progress in measuring the source counts of potential ALMA calibrators at higher frequencies.

2.3 The Fast Switching Schematic

Following the lead of D'Addario (2003) in the analysis of the the instrumental sequence, we present a rather detailed picture of the sequence of observing operations that will be required of ALMA in dual-frequency fast switching phase calibration in Figure 1. A number of terms in this heuristic description of fast switching, some of which are important in the evaluation of fast switching in Section 7 are explicitly defined in Appendix A. This figure shows the instrumental sequence (or cross-band calibration), a moderate number of target sequences (simple fast switching cycles, which is all we need if we observe the calibrator at the target frequency), and, before the instrumental phase has drifted significantly, a final instrumental sequence. We call the instrumental sequence followed by several target sequences a single major cycle.

The major cycle time is set by the instrumental stability time scale, which we assume in this work to be 300 s. While the simulations in this memo do not include any instrumental delay errors, they will indicate how large the instrumental delay errors can be without seriously degrading ALMA's performance while fast switching. Of course, we hope the instrumental stability time scale is longer than 300 s, as it should be at moderate to low frequencies. If the instrumental stability time scale is longer, our work is still valid as a lower limit for the overall fast switching efficiencies.

Conceptually, fast switching starts before the observations begin. We must have good knowledge of the fluxes and positions of potential calibrator sources for both the target and instrumental sequences. Given database of potential sources, possibly updated with recent observations to provide current fluxes, we determine the optimal calibrators for both the target sequence and the instrumental sequence (these calibrators will usually be different). It would

take just over 1.5 s per potential calibrator to slew to and measure the flux of each potential target sequence calibrator as the time is dominated by the slew time and these sources will tend to be of order a degree apart. The brighter, more distant instrumental sequence calibrators will take longer to observe because they are farther away.

During a single 300 s major cycle, we perform a short (10-25s) instrumental sequence on a bright (ie, 0.5 - 1.0 Jy) and relatively distant (5-15 deg) calibrator, followed by several (10-20) cycles of the target sequence, alternating between the target source and a very close (< 2 deg) moderately bright (0.05 - 0.2 Jy) phase calibrator. In the schematic, observations at the target frequency are unshaded, observations at the calibration frequency are shaded black, and slewing is shaded with diagonal lines. The majority of the time is spent on the target source at the target frequency. The calibrator observations in each target sequence cycle are very short, and the instrumental sequence calibrator observations which bracket the 300 s major cycle are also very short.

In the instrumental sequence, we begin by slewing to the really bright calibrator source which we must accurately detect at both the cal and the target frequencies. A bright source minimizes the detection time and hence minimizes the residual atmospheric phase errors which blow by in the time between calibrator and target frequency observations. With ALMA's sensitivity, these sources can easily be detected with sufficient SNR at the calibration frequency in 1 s. It will take 1.5 s to change to the target frequency. As we are racing the atmosphere and we don't have to change sky positions, any reduction in the time required to switch frequencies (ie, shorter than the 1.5 s specification) will be beneficial – in fact, the atmospheric error made in the instrumental sequence will ultimately set the requirements on the magnitude of the acceptable long-term electronic phase drift. Often, this calibrator source will also be bright enough to adequately detect the phase at the *target frequency* in a single 1 s integration, in which case we finish the instrumental sequence by slewing back and performing several target sequences. If the instrumental sequence calibrator is not bright enough, we will need to switch back and forth between cal frequency observations and target frequency observations until we obtain high enough SNR on the phase solutions at the target frequency. We perform this frequency switching on the instrumental sequence calibrator to remove the contribution of atmospheric phase errors on time scales greater than about 2 s, essentially calibrating the target frequency observations of the instrumental calibrator with the cal frequency observations of the same source.

In a single target sequence, (which was formerly all we considered in our model of a fast switching cycle, and will sometimes be referred to in this work as a fast switching cycle), we start with a short calibration observation at the calibration frequency. The integration time on the calibrator is determined by the calibrator's strength, ALMA's sensitivity, and the signal-to-noise ratio (SNR) required to scale the calibrator's phase solutions to the target frequency and still have errors which are less than the residual atmospheric phase errors. In all of our simulations, this is always less than a second. The required SNR is set by the requirement that the thermal noise, converted into a phase at the target frequency, be small compared to the atmospheric phase contribution. This small thermal noise contribution to the phase is added into the final rms phase.

After we detect the phase on the calibrator with sufficient SNR, we slew from the calibrator to the target source. The specification for antenna motion is 1.5 deg in 1.5 s, which is a typical distance to a calibrator. Furthermore, the specification on the setup time to change frequencies is 1.5 s, which will happen during the slew. In our modeling of the antenna slewing (Holdaway,

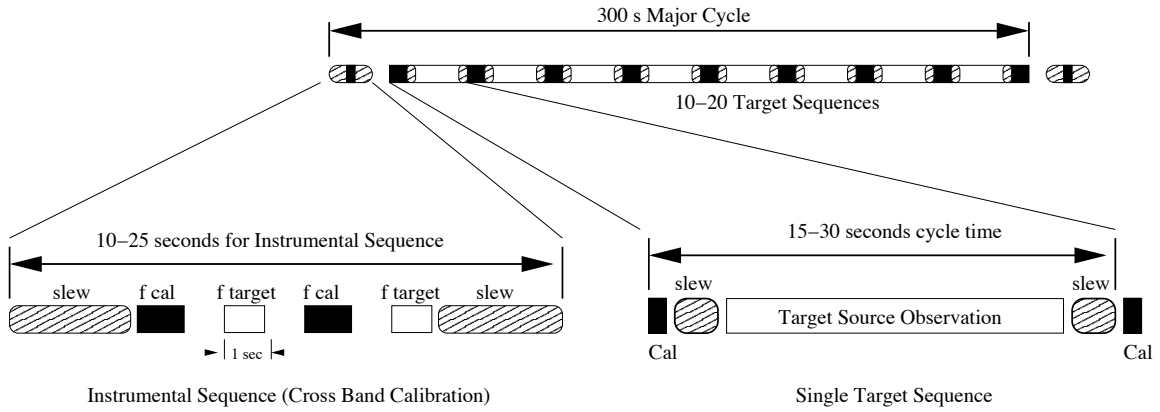

Figure 1: Overview of fast switching, showing both the target sequence and the instrumental sequence. The calibrator for the target sequence will typically be within 2 deg of the target source, while the calibrator used in the instrumental sequence will be up to 15 deg away from the target source.

2001 – with a correction by capping the maximum slew speed for long slews which will be required for reaching the more distant instrumental sequence calibrator), it appears that very short slews (like 0.25 deg) might be completed in somewhat less than 1.5 s, so if we are able to change frequencies in less than a second, we'll take advantage of that capability here too. After slewing onto the target source with a specified pointing error of less than 3 acrsec (which will probably not be acceptable for very high frequencies or mosaicing – more on this topic below), we begin the actual observations on the target source at the target frequency. After integrating on source at the target frequency for 10-25 s, which is determined by a global optimization of the entire fast switching phase correction procedure considering the current atmospheric conditions, the characteristics of the optimal calibrator, and the cal and target frequencies, we again slew back to the calibrator, and as we reach the calibrator, here ends a single target sequence.

Most often, we would immediately follow this target sequence with several more, starting on the phase calibrator again. If this is the last target sequence before another instrumental sequence, we should throw in a final observation of the calibrator to facilitate phase interpolation. If we are about to end the source block, or go off and do another sort of calibration, we should throw in a final instrumental sequence to facilitate in interpolating the scaled instrumental phase difference.

2.4 What About Fast Switching While Mosaicing?

ALMA antennas have a 0.65 arcsec pointing error specification to permit accurate mosaic imaging and good single pointing sub-millimeter performance (sub-millimeter mosaicing will be somewhat compromised by this pointing). So, what is the logic behind the 3 arcsec pointing specification for fast switching? It was originally reasoned that fast switching would do little to improve phase fluctuations on baselines shorter than 200 m (ie, $vt/2 + d$), and further reasoned that most mosaicing would be performed in the compact configurations with baselines less than 200 m. In these short configurations, the native phase stability of the atmosphere would permit

observations without fast switching.

However, since conceiving of this fast switching spec, ALMA has grown in collecting area, and the smallest configuration is almost 200 m, while the effective switching scales can indeed be less than 200 m. Furthermore, often mosaics will be made in larger configurations which do require phase calibration. And last, this specification was originally just a factor of 3 worse than the mosaicing pointing spec of 1 arcsec for the MMA's 8 m antennas – when we increased ALMA's antennas to 12 m, we tightened the mosaicing pointing spec but forgot to tighten the fast switching pointing spec, so now fast switching's pointing is a factor of 4.6 off of the static pointing spec. So, what can we do?

We do not have a spec for how long it will take ALMA antennas to settle to the 0.65 arcsec pointing level after fast switching, so we will have to study the antenna's settle down capabilities carefully to address this issue. Basically, when mosaicing and fast switching simultaneously, we will probably need to wait longer while the antennas slew to the target source to permit them to achieve better pointing. How much better pointing and how long will depend upon the required mosaic image quality, and in turn, on the mosaic's SNR. We will often be able to permit larger pointing error on the calibrator, except at the higher frequencies. The time lost to waiting for the antennas to achieve superior pointing for mosaicing has not been included in the analysis of the fast switching efficiency, but should be included after we have studied this issue on the prototype antennas.

2.5 What About Fast Switching While Observing at Sub-millimeter Wavelengths?

The same issue will cloud our observations of sub-millimeter wavelength sources. Even single pointing sub-millimeter observations will require excellent pointing on the target source, so more time will be lost waiting for the antennas to settle to the desired pointing, which will depend upon both the observing frequency and the required image quality.

3 Analysis of Fast Switching

3.1 RMS Phase Jitter, Phase Errors, and the Structure Function

To estimate the residual phase errors after fast switching, we have in the past used the expression

$$\sigma_\phi = \sqrt{D_\phi(v_{atmos} t_{cycle}/2 + d)}, \tag{1}$$

where σ_ϕ is the rms residual phase error, D_ϕ is the phase structure function determined by the site testing interferometer (Radford, 1996; Holdaway et al, 1995), v_{atmos} is the velocity of the atmosphere at the height of the turbulent layer, t_{cycle} is the fast switching cycle time, and d is the linear distance between the lines of sight to the target source and the calibrator, at the altitude of the turbulent layer. This quantity represents the standard deviation of the residual phase within a single target sequence.

In the data analysis of the site testing interferometer data, we perform a power law fit to the root structure function, and parameterize it as

$$\sqrt{D_\phi(\rho)} = a \cdot \rho^\alpha,$$

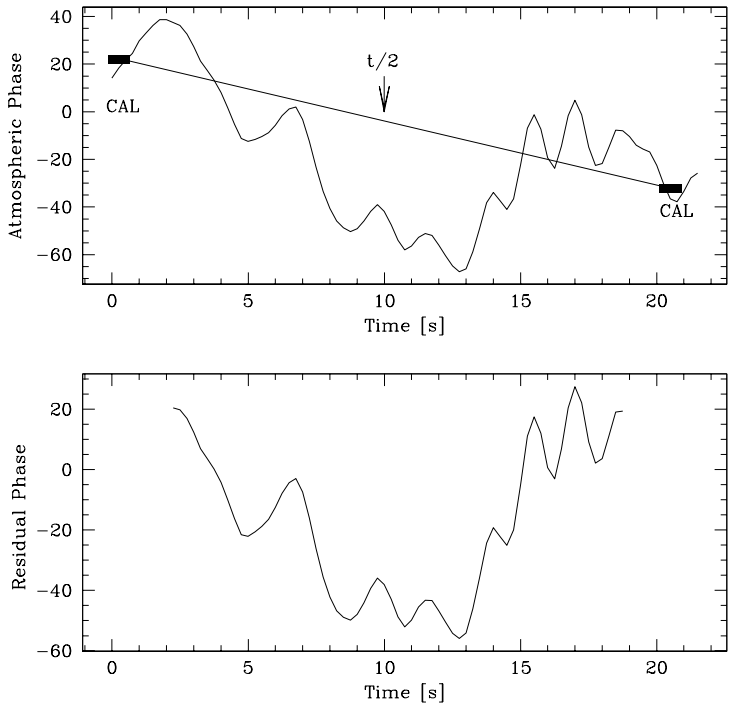

Figure 2: Most of the fast switching cycle will be closer to a calibration observation than $t_{cycle}/2$. Hence, the phase errors will be somewhat less than $\sqrt{D_\phi(vt/2+d)}$; the d term is generally small compared to $vt/2$.

where a is, in rough terms, the amplitude of the atmospheric phase fluctuations, and α is the root phase structure function power law exponent. The median value of α, for six years of site testing at Chajnantor, is 0.58.

In the term $v_{atmos}t_{cycle}/2 + d$, the d ends up being negligible: with v_{atmos}=12 m/s and t_{cycle}=20s, $vt/2$ will typically be 120 m. For a distance between calibrator and target source of 1 deg and a height of the turbulent layer of 500 m above the ground, d ends up being less than 10 m for a source at the zenith (lower elevation angles will make d somewhat larger). In the reasoning below, feel free to conceptually ignore d, although we did include d in the simulations.

The expression in Equation 1 systematically overestimates the residual phase error which will occur in fast switching. Figure 2 illustrates the problem. The top graph shows the simulated uncorrected atmospheric phase time series for a 1000 m baseline interferometer, and the lower graph shows the residual phase as a function of time on the target source after correcting with linear interpolation. Some time is lost on the lower plot due to calibration observations and slewing. These plots only show the effects of the atmosphere, as the source visibility phase and instrumental phases have not been included.

With yet another home grown AIPS++/glish tool, `vtdsim.g`, we have a laboratory to explore the finer details of fast switching and better determine the relationship between the

residual phase, the phase structure function, and the effective fast switching baseline $vt/2 + d$. From performing such detailed simulations of fast switching and the statistics of the resulting residual phases, we have identified three effects which we need to address to more accurately gauge the success of our full blown simulated fast switching observations which are presented later in this memo:

- The rms residual phase error, given by the rms of the residual phase time series (the lower graph in Figure 2), will be a valid number for calculating decorrelation losses. However, the average phase error made on the target source visibility will be much smaller. In this case the rms residual phase is 25 deg, while the mean phase error on this integration will be -17 deg. In our analysis, we will consider both the rms residual phase error for purposes of decorrelation calculations, and the rms of the average phases, for purposes of visibility error calculations.

- the rms phase error at the center of the target source integration (ie, 10 s, or $t_{cycle}/2$) might appropriately be estimated by the root structure function evaluated at $vt/2$, but most of the target source integration will be significantly closer to one or other calibration observations. In Figure 2, the largest residual phase errors on the target source observation occur between 8 and 13 s, and the phases near the calibrations are much smaller.

- For a root structure function exponent α of 0.58, linear interpolation will provide a marginal improvement over a "closest calibrator" interpolation. For flatter α (ie, more like white noise), linear interpolation could actually be worse than closest calibrator interpolation, and for steeper α (ie, up to the maximum theoretical value of 0.83), linear interpolation should significantly reduce the residual phase. **Hence, the interpolation method should depend upon the details of the atmospheric conditions.**

Including these three factors in simulations (mean vs rms phase, interpolation improvements, and $vt/2$ being the worst case), we simulated fast switching observations through a model atmosphere with linear interpolation, and we empirically determine that the rms phase error is indeed less than the the phase structure function evaluated at $vt/2 + d$, reduced by a factor $\gamma_0(\alpha)$ (we have not demonstrated any dependence upon α, but it is reasonable):

$$\sigma_\phi = \gamma_0(\alpha) \cdot \sqrt{D_\phi(v_{atmos} t_{cycle}/2 + d)}, \tag{2}$$

and the rms of the phase errors averaged over each target integration can be written as the phase structure function reduced by $\gamma_1(\alpha)$:

$$\sigma_{\bar{\phi}} = \gamma_1(\alpha) \cdot \sqrt{D_\phi(v_{atmos} t_{cycle}/2 + d)}. \tag{3}$$

We expect the γ factors to be weak functions of α, though at this time we have not performed exhaustive studies. For the simulations we performed, with $\alpha = 0.58$, and $t_{cycle} = 20$s, we find that $\gamma_0 = 0.65$ and $\gamma_1 = 0.35$

If you observe with a single interferometer through the atmosphere with phase errors, the rms phase (after subtracting out the average phase) will increase with integration time until, after many "crossing times" (ie, the baseline length divided by the atmospheric velocity), the rms phase will saturate. When we worked out the site testing interferometer data reduction

pathway (Holdaway et al, 1995), we performed this analysis, looking at how the rms phase increased with integration time. The rms phase reached a plateau at about 10 minutes, and then started to increase again for longer integration times. We interpreted this to mean that 10 minutes integration resulted in a saturated phase, and beyond 10 minutes, phase errors from thermal changes in the cables or satellite motion came into play.

However, our simulations with `vtdsim.g` indicate that a 600 s integration on a 300 m baseline and a 12 m/s wind is not really enough to reach saturation. When simulating a 300 m baseline interferometer with the `vtdsim.g` machinery, we find that the rms phase only accounts for about 0.70 of the phase structure function at 300 m. It is unclear if reanalysis of the site testing interferometer data using a longer integration time is the right thing to do, as non-atmospheric phase errors will creep in. For now, there is a very simple fix we can apply, and that is to incorporate this correction factor, 1/0.70, into the γ factors:

$$\gamma_0' = \gamma_0/0.70 = 0.93$$

$$\gamma_1' = \gamma_1/0.70 = 0.50$$

One more detail we must address is the way the phase errors will average down over several fast switching cycles. That γ_1' is 0.50 indicates that the standard deviation of the average phases over several switching cycles will be significantly lower than the rms phase. Typically, we will perform 10-20 such fast switching cycles, and, as the residual atmospheric errors after fast switching calibration are random, and the noisy gain errors on the fast switching calibrator are random, averaging the target source visibilities from several fast switching cycles will result in better and better estimates of the visibility phase. We assert that the ensemble average of the mean phase error after N_{cycles} fast switching cycles will go approximately as

$$\langle\bar{\phi}\rangle = \gamma_1'(\alpha)/\sqrt{N_{cycles}} \cdot \sqrt{D_\phi(v_{atmos}t_{cycle}/2 + d)}.$$

This assertion relies upon the N_{cycles} being independent. The crossing time of long baselines will be much longer than the target sequence cycle time, so each switching cycle will not be strictly independent. However, the fact that new atmosphere is coming into view (at least on one antenna) with each new cycle, and the randomizing influences of interpolation, should result in the the average phases for each cycle being largely independent.

One final point concerning the number of visibilities which can be averaged is the crossing time of a visibility across a Nyquist sampled (u,v) cell due to earth rotation. The size of the (u,v) cells is set by the inverse of the field size we are imaging, and the number of cells will be proportional to the baseline length. Long baselines will zip across the (u,v) cells very quickly, short baselines will move through the cells slowly. The crossing time sets an upper limit to the amount of time one can average the visibilities for.

For full primary beam imaging, the (u,v) cell crossing times are given in Table 1.

3.2 Error Analysis of Fast Switching

We start here by analyzing the phase errors made in fast switching in the case that the calibration is performed at the same frequency as the target source is observed at. In this case, no instrumental sequence calibration needs to be performed. The phase jitter, appropriate for calculations of decorrelation, is then given by Equation 2, and the mean phase error in a single fast switching cycle is given by Equation 3.

Baseline [m]	t_{int} [s]	N_{cycles}	$\gamma_1'/\sqrt{N_{cycles}}$
200	412	20	0.11
400	206	10	0.16
1000	82	4	0.25
2000	41	2	0.35
4000	20	1	0.5
10000	8	-	-

Table 1: The (u,v) cell crossing time for full primary beam imaging, for a baseline of the specified length, and the approximate number of fast switching cycles which could be averaged and the reduction factor in the phase error due to averaging. If only a portion of the primary beam were being imaged, the (u,v) cell sizes would be larger, the crossing time longer, and more averaging could take place, so these numbers represent a worst case.

Next, following D'Addario's memo (D'Addario, 2003), we analyze the errors made in fast switching for the case where the target frequency ν_t and the calibration frequency ν_c are different.

3.2.1 Target Sequence

By scaling the calibrator phase ϕ_{cal} by the ratio of the frequencies and subtracting that from the target phase ϕ_{tar} (ie, we are ignoring dispersive effects), we get

$$\phi_{tar} - \left(\frac{\nu_t}{\nu_c}\right)\phi_{cal} = \phi_{tar}^{true} + \phi_i(\nu_t) - \left(\frac{\nu_t}{\nu_c}\right)\phi_i(\nu_c) + \gamma_1 2\pi\nu_t\sqrt{D_\tau(vt_{t.s.}/2 + d)} + \left(\frac{\nu_t}{\nu_c}\right)\epsilon_c \quad (4)$$

where ϕ_{tar}^{true} is the true target source visibility at the target frequency, which can be ignored in this analysis, the ϕ_i terms are instrumental phases (assumed here to be constant, or at least small compared to other problematic phases), $D_\tau(vt_{t.s.}/2 + d)$ is the *delay* structure function (ie, the phase structure function, cast into a frequency-independent form as delay), $t_{t.s.}$ is the cycle time for the target sequence, and ϵ_c is the phase error on the calibrator gain solution due to thermal noise. ϕ_{tar} is the phase of a single baseline's visibility, but to reduce the noise contribution, ϕ_{cal} is synthesized by solving for the antenna-based gains at the calibration frequency (ie, an improvement in SNR by $\sqrt{N-2}$), and then differencing two antenna-based phases (ie, a loss in SNR of $\sqrt{2}$ to result in an overall gain of $\sqrt{(N-2)/2}$) to give the high SNR estimate of the calibrator visibility phase at the calibration frequency.

3.2.2 Instrumental Sequence

We define the scaled instrumental phase difference Φ_i to be

$$\Phi_i = \phi_i(\nu_t) - \left(\frac{\nu_t}{\nu_c}\right)\phi_i(\nu_c). \quad (5)$$

We can estimate Φ_i by performing a quick two-frequency observation a calibrator source which is bright at both the target and calibrator frequencies and forming the scaled phase difference, but this estimate will be contaminated by both atmospheric phase errors which occur on that

short time scale while the observing frequency (but not the source) changes, and thermal noise due to the short observations intended to minimize the atmospheric errors:

$$\hat{\Phi}_i = \phi_{tar} - \left(\frac{\nu_t}{\nu_c}\right)\phi_{cal} \quad (6)$$

$$= \Phi_i + \gamma_1 2\pi\nu_t\sqrt{D_\tau(vt_{i.s.}/2)} + \sqrt{\frac{\epsilon_t^2 + \left(\frac{\nu_t}{\nu_c}\right)^2\epsilon_c^2}{N_{i.s.}}}, \quad (7)$$

where $t_{i.s.}$ is the time between the center of the target frequency observation and the center of the cal frequency observation in the instrumental sequence (taken in our analysis to be 2 s), and $N_{i.s.}$ is the number of instrumental sequence integrations that must be performed to reach the required SNR. ϵ_t is the phase error due to noise in the gains at the target frequency.

How much time do we need to detect $\hat{\Phi}_i$, or how do we calculate the noise in the final term? We need to synthesis each baseline-based $\hat{\Phi}_i$ from the antenna-based gains at the two frequencies, as we did in the target sequence, to get higher SNR. However, we may still need more SNR on $\hat{\Phi}_i$. To get that SNR, we can't just integrate longer, because then we would be dominated by the atmospheric residuals. To minimize the atmospheric phase errors, we use very short (ie, 1 s) integrations at the calibration and target frequencies and change between the frequencies as fast as we can (the specification is 1.5 s, and we are hoping for 1 s). The cycle time for the instrumental sequence measurement, $t_{i.s.}$, will be twice the integration time plus twice the frequency change time. We can remove the effects of the atmosphere on time scales of $t_{i.s.}/2 \simeq 2$ s by forming the scaled phase difference, or $\hat{\Phi}_i$, with the lower-than-desired SNR phase data that we get from a single pair of 1 s measurements at the two frequencies. If we need higher SNR, then we need to perform this measurement cycle multiple times and average each value of $\hat{\Phi}_i$ until the SNR improves sufficiently. In order to keep the noise in the scaled phase difference well behaved, we should probably represent $\hat{\Phi}_i$ as the phase of a complex number, and average the complex numbers, and the take the final phase.

We assume that the atmospheric phase errors and the thermal noise are statistically uncorrelated, so the rms error phase fluctuations are given by adding the atmospheric term and the noise term in quadrature.

4 Calibrator Source Count Estimates

In order to calculate the t_{cycle} to evaluate fast switching, we need to know t_{cal} (the integration time on the calibrator) and t_{slew} (the slew time to and from the calibrator), so we need to know how bright and how far away the calibrator sources are likely to be.

4.1 What Sources Are Possible Calibrators?

The success of fast switching is dependent upon an adequate supply of moderately bright calibration sources close by to the target source. The main population of calibrators for fast switching is the flat spectrum quasars. SiO masers have been suggested, but there are not enough of them which are bright enough to make a significant impact on our need for calibrators (Holdaway, 1996). Ultra compact HII regions have also been considered, but they are extended and there probably aren't enough either (Holdaway, 1996, unpublished). Recently, Butler (2003) has suggested using thermal dust emission from distant galaxies at high frequencies

where they will dominate the sky (rather than calibrate sub-millimeter observations at 90 GHz), but these sources will be extended (approximately 1 arcescond), and are probably not optimal for phase calibrators. Hence, we restrict the analysis of calibrators to the flat spectrum quasars. Adding any other population of sources to the calibrator pool will only improve the efficiency of fast switching, so our work will stand as a valid lower limit to fast switching's performance.

Butler's work does raise an interesting question. If we perform the fast switching phase correction at the same frequency as the target source observations, the target sequence solves for both the atmospheric and instrumental delays, and we bypass the instrumental sequence (and any associated errors). Logically, at low target frequencies where the quasar fluxes are high and the ALMA sensitivity is good, it should be optimal to perform the fast switching phase calibration at the target frequency. At high target frequencies where the quasar fluxes are falling and ALMA sensitivity is poor, it will be advantageous to perform the fast switching calibration at a lower frequency and scale the solutions to the target frequency. So, there will be a frequency below which we will perform the phase calibration at the target frequency, and above which we will perform the phase calibration at 90 GHz and scale the solutions up. What is that magic frequency?

To answer this, as well as to investigate the instrumental sequence, we need to estimate the quasar source counts at each ALMA band.

4.2 Estimating Flat Spectrum Quasar Source Counts in the Millimeter and Sub-millimeter

Figure 3 shows the histogram of the spectral index ($S(\nu) \propto \nu^{-\alpha}$) distribution from 8 GHz to 90 GHz for the 367 flat spectrum quasars observed by Holdaway, Owen, and Rupen (1994). (Our apologies for reusing the symbol α for both the quasar spectral index and the atmospheric structure function exponent, but the context should indicate which concept we are using.) The 8 GHz core fluxes were measured by Patnaik *et al.* with the VLA in A array. The 90 GHz fluxes were measured at the NRAO 12 m. Under the assumption that any extended emission is steep spectrum and will be negligible at 90 GHz, we posit that this spectral index distribution describes the quasar cores. We found that the spectral index distribution did not depend upon the quasar flux, so we used all 367 quasars to determine a single spectral index distribution using Feigelson's ASURV code (Feigelson, 1985).

We have also performed a two Gaussian fit to this histogram (dotted lines, the sum of which is the dashed line). The black boxes represent the integral of the summed Gaussian fit over the histogram boundaries, appropriately normalized for comparison to the histogram. Because the number of degrees of freedom in the fit (6) is about the same as the number of independent data points in the histogram (7), we expect a very good fit. We have used the Gaussian fit, rather than the 7 bin histogram, for our extrapolations of source counts to the higher frequencies, as the sharp edges were causing some odd bumps in the source counts extrapolations.

Starting with the source counts of flat spectrum quasars at 5 GHz (Condon, 1984), we modulated the fluxes of these counts by the core fraction distribution of the 3CR2 flat spectrum sources, so that the modified counts represented the source counts of only flat spectrum cores, ignoring extended components. We further modulated the source counts by the flat spectrum quasar spectral index distribution between 8 GHz and 90 GHz which we determined, following the prescription by Condon (1984) to scale the source counts up to 90 GHz.

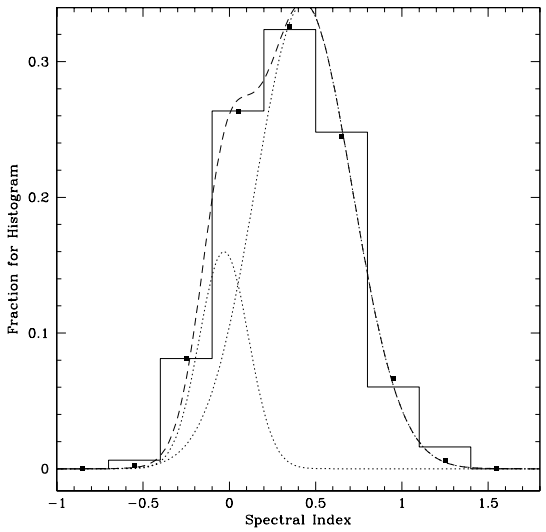

Figure 3: The seven bin histogram is the spectral index ($S(\nu) \propto \nu^{-\alpha}$) distribution from 8 GHz to 90 GHz for the 367 flat spectrum quasars observed by Holdaway, Owen, and Rupen (1994). See the text if you want to know about the Gaussians and filled squares.

At frequencies above 90 GHz, the quasar cores are expected to become optically thin, which will result in a spectral steepening. Hence, for frequencies above 90 GHz, we assume that the sources have a spectral break and we steepen the entire spectral index distribution by 0.5 when estimating quasar source counts at frequencies above 90 GHz. This steepening results in a median spectral index of 0.8 at frequencies about 90 GHz, which appears to be reasonable to several famous radio astronomers (Frazer Owen, Richard Hills, and Robert Laing; private communications). The resulting integral source count estimates, including the spectral steepening above 90 GHz, are displayed for a range of frequencies in Figure 4.

We have written an AIPS++/glish tool, `sourcecountsim.g`, which performs the frequency scaling of the source counts and can simulate a calibrator field which is consistent with the estimated source counts and spectral index distribution. The `sourcecountsim.g` code is not part of the AIPS++ distribution, but can be obtained from Mark Holdaway's home page at `http://www.tuc.nrao.edu/ mholdawa/`, along with other software used to perform the calculations in this memo.

5 What Frequency Should We Calibrate At?

As mentioned above, the default scheme for fast switching is that we will calibrate at 90 GHz and scale the phase solutions up to the observing frequency. There are two issues which pertain to the assumption of calibrating at 90 GHz which we need to address now.

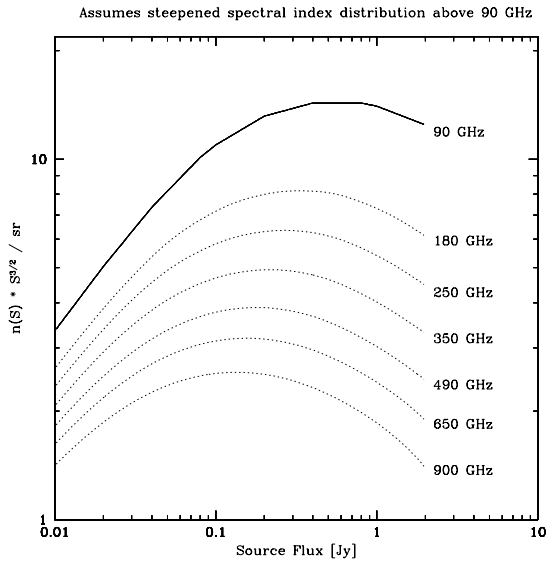

Figure 4: These are the integral source counts of flat spectrum quasars at various ALMA frequencies. The counts at 90 GHz will be fairly accurate, but we are guessing at the spectral index distribution for higher frequencies: to estimate the higher frequency source counts, we are taking the measured 8-90 GHz spectral index distribution and steepening it by 0.5, resulting in a median spectral index of 0.8 above 90 GHz.

5.1 Is 90 GHz the Optimal Calibration Frequency?

We have not examined this in detail yet (!), and we should, just to cover our bases. If dual-frequency fast switching is to be used, band 3 is probably the best frequency for the calibration. We *have* investigated which frequency is optimal for pointing calibration at the ATF (Holdaway and Mangum, 2001), and the combination of the decent sensitivity and the "lever arm" of the smaller beam at the higher frequency makes 90 GHz superior to 30 GHz for pointing determinations. There are similar arguments for fast switching phase correction that have not been entirely spelled out.

What about performing the calibration observations at higher frequencies, like 140 GHz, and scaling up to the target frequency? Answering this question would probably be dominated by our assumptions about how the calibrator fluxes are falling down, and it is probably not worth investigating this question at this time.

When the final ALMA systems are in production and we understand the system temperature as a function of frequency, we can determine the optimal frequency band within band 3 for fast switching.

5.2 Potential Issues with Instrumental Sequence Calibration Sources

We have asserted that the instrumental sequence will be performed on a quasar which is bright at both the calibrator frequency and the target frequency. The success of this strategy depends, among other things, on the quasar looking the same at the calibration and the target

frequencies. This may not be the case.

For example, as dust emission increases in flux with frequency, the quasar point source may be surrounded by extended dust emission. The dust emission problem probably doesn't exist for moderate frequencies, perhaps only for frequencies of 400 GHz and above. If the dust emission is symmetric and centered on the quasar, it won't contribute to the phases. Furthermore, if we are observing in a very large configuration, much of the dust emission could be resolved out – in other words, a (u,v) range could be determined observationally in which the calibration source was well approximated by a point source. Such a (u,v) range would eliminate some baselines from the phase solution, thereby requiring a brighter calibrator or more integrations on the calibrator.

Another potential problem is that the position of the quasar core will depend upon the frequency. As we observe at higher frequencies, the region at which the jet becomes optically thick (functionally "the core") will be closer and closer to the central engine. If the position difference with frequency is large enough, this would introduce a systematic error in the instrumental sequence. We need to investigate how large this systematic error might be.

5.3 Dispersive Phase, Dry Fluctuations, and Implications on the Calibration Frequency

We claim that we can scale the phase solutions from the calibrator frequency up to the target frequency simply by multiplying by the ratio of the frequencies. This is only true for target frequencies at which the atmosphere is non-dispersive, or up to about 350 GHz. However, at sub-millimeter wavelengths, the atmosphere is dispersive enough to result in significant deviations from this simple phase scaling (Holdaway and Pardo, 2001). At the very least, we will be required to employ radiation transmission codes such as ATM to instruct us in the proper phase scaling from calibrator to target frequencies. However, we could be limited in the accuracy of the transmission codes, or we may be limited in our knowledge of physical atmospheric parameters such as the temperature profile or the water vapor profile, which would result in some errors in our prescribed phase scaling. We can study the latter question now using ATM with various atmospheric profiles. In this memo we do not attribute any errors to the phase scaling process.

However, we must consider the possibility that the dispersive phase in the sub-millimeter range may not permit fast switching to accurately scale the phases from calibration to target frequency. If this were the case for certain frequencies or certain atmospheric conditions, we would have to resort to performing the fast switching calibration at the target frequency and make do with the weaker or more distant phase calibrators. But again, the calibrators may have dust structure at the higher frequencies and may not be appropriate for calibrating at the target frequency when observing in the sub-millimeter. Later in this memo, we document how effective fast switching is at each target frequency, and it is not much worse than calibrating at 90 GHz.

While the dry component of the atmosphere results in the largest portion of the overall atmospheric delay, we expect that the dry atmosphere will be relatively stable and will contribute essentially none of the phase fluctuations. If there are significant phase fluctuations introduced by fluctuations in the dry atmosphere, fast switching with different calibration and target frequencies will still work fine unless there is a significant dispersive phase. In other words, if there are dry phase fluctuations, we can calibrate at 90 GHz and scale the phase up

to about 350 GHz, but we we can't scale the phase up to the sub-millimeter where the phase is dispersive – basically, we would need to know how much of the phase errors are dry and non-dispersive and how much of the phase errors were wet and dispersive. So, if dry fluctuations were significant, sub-millimeter observations using fast switching phase correction would need to observe the calibrator at the target frequency.

6 Our Method of Calculating the Residual Phase Errors

6.1 This is a "squishy" sort of problem

Fast switching is a very complex multi-dimensional system. The variables that are out there include: the inherent sensitivity of the telescope, the distance to the calibrator, the strength of the calibrator, how much time we spend calibrating (multiply the last three dimensions by two, as there are both the target sequence calibrators and the instrumental sequence calibrators), how much time we spend observing our target source before we go back and observe the calibrator again, the nature and level of the atmospheric phase fluctuations, and the velocity of the turbulent layer. With so many dimensions, the overall fast switching system becomes rather " floppy" – if one dimension of the problem becomes much harder (say we discover that the 90 GHz calibration sources are only half as bright as we had assumed), the impact of that change becomes absorbed in several dimensions (we go a little bit further away to reach a somewhat better calibrator, integrate a bit longer, shorten the overall cycle time, which decreases the on-target-source duty cycle), resulting in a final result, the overall observing efficiency, which is only marginally reduced.

The one exception to this seems to be the atmosphere. If you make the atmosphere twice as bad, the lost observing efficiency (due to both time lost to calibration and to phase decorrelation) gets twice as large.

6.2 Monte Carlo Simulations

Our job is to estimate how well fast switching phase correction will work. This is a messy, multi-dimensional problem, and we must consider

- varying and largely uncorrelated atmospheric opacity and phase fluctuations
- observations at frequencies ranging from 35 to 900 GHz
- variation of the quality of the calibrator field around the target source: some targets will have fortuitously bright quasars very close by, other targets will not have a good calibrator very near. Additionally, each calibrator source will have a different spectral index, so some really good calibrators at 90 GHz will be useless for the instrumental sequence.
- variation in the velocity of the moist turbulent layer, which we ignore by taking it to be 12 m/s.
- variation in the height of the turbulent layer, which we simply take to be 500 m. The turbulent height only comes into play with the term d, the linear distance between the lines of site to the cal and target sources at the height of the turbulence. As d ends up being essentially negligible, any error in this height will have very little effect.

Freq [GHz]	Band	tau at 225 GHz	phase [deg]
unused	0	0.101	11.44
43	1	0.220	6.71
80	2	0.129	5.44
90	3	0.129	3.635
145	4	0.089	2.955
190	5	0.060	3.210
230	6	0.056	2.175
345	7	0.045	1.840
500	8	0.037	1.615
680	9	0.032	1.155
880	10	0.025	0.790

Table 2: Median values of the 225 GHz opacity and the 11.2 GHz, 300 m baseline site testing interferometer rms phase allocated to the ten ALMA observing bands.

As we have done in the past (Holdaway, 2001; Holdaway 2003), we reduce the dimensionality of this problem by matching the observing frequency to the atmospheric conditions to simulate the results of dynamic scheduling. Unlike Holdaway 2001, but similar to Holdaway 2003, we consider both the opacity and the phase stability in splitting up the atmospheric conditions among the observing bands. So, while the best opacity and stability conditions from the joint distribution will go to band 10, we have fallen short of a fully-optimized analysis (ie, picking those remaining atmospheric conditions that truly optimize the sensitivity at each observing band). We have thrown out the worst 20% of observing conditions as unusable (in retrospect, this is a bit extreme, and we could have thrown out 10-15%), and have assumed that each band will be used for 8% of the time. The median values for the 225 GHz opacity and 11.2 GHz/300m site testing interferometer for the conditions allocated to each observing band are shown in Table 2.

The only remaining dimensions of the problem we must worry about are the calibrator fluxes, the proximity of the calibrators to the target source, and the calibrators' spectral indexes. (In general, we have to find two calibrators for each target source, one for the target sequence, and one for the instrumental sequence.) We deal with the calibrator properties by performing Monte Carlo simulations of representative calibrator fields 40 deg by 40 deg. The source counts in each calibrator field is consistent with the 90 GHz source count estimates we address above, and the spectral index distribution is the one measured from 8 to 90 GHz, steepened by 0.5 above 90 GHz. We have created 1000 such calibrator fields, and we use the same fields for each different observing frequency or atmospheric conditions so that the fast switching results don't depend upon variations in the underlying calibrator source fields. For each observing scenario (ie, target frequency, calibration frequency, and atmospheric conditions), we simulate a fast switching observation for each of the 1000 calibrator fields, selecting the calibrator sources which result in the maximum efficiency for the fast switching observation. This process gives rise to 1000-element distributions of optimal target sequence calibrator flux, optimal efficiencies, optimal residual phase errors, etc. Median values of these distributions are reported below.

Using the same simulated calibrator fields for each different observing scenario will have the affect of reducing noisy scatter in the results among the different target bands so relative conclusions are not affected, but will also increase any systematic errors as the entire ensemble of simulations will suffer from them – but with 1000 different instantiations of the millimeter calibrator sky, the systematics should be small.

The simulations which we report on here were carried out in AIPS++/glish which a suite of tools developed for ALMA work:

- **drivefast.g** drives the simulation tool for the specific cases we studied and implements the Monte Carlo aspect of the simulations.
- **fastswitchsim2.g** encodes the essential logic of selecting the optimal calibrator and calculating the residual phase errors and efficiencies.
- **sourcecountsim.g** simulates fields of calibrators consistent with specified source count statistics and spectral index distribution, and also shifts source counts in frequency.
- **stidata.g** encapsulates transforming the site testing data to other frequencies and baselines.
- **almasensitivity.g** is used to calculate the noise level of a certain observation or the amount of time that is required to reach a certain noise level.
- **almatau.g** encapsulates the opacity characteristics of the atmosphere above the ALMA site.

These glish tools can be found at `http://www.tuc.nrao.edu/ mholdawa/`

7 Results

We present the quantities that are defined in Appendix A, as calculated with our Monte Carlo simulations, in Tables 3 through 5. The γ' factors have been included in calculating these results. Table 6 deals with the 5th percentile atmospheric phase and opacity, and is specifically included so we can derive specifications for the electronic phase fluctuations. These tables show the median values of the various parameters calculated in the simulations.

The units of the quantities in these Tables are: targetfreq, calfreq [GHz], el [deg], rms300 (site testing phase) [deg], phases and gainerror [deg], calflux [Jy], caldist [deg], tslew, tcal, tcycle, ttarget, toverhead [seconds]. Efficiencies are noise-like quantities, as opposed to time-like quantities. The overal efficiency, eff0, is the product of the eff1, the square root of the duty cycle, and eff2, which id just the decorrelation from residual phase errors.

These tables are sort of sideways so many relevant terms can be shown. There are a number of interesting results:

- Things are really very demanding in the sub-millimeter, with typical overall efficiencies (all eff0) of about 0.70; total residual phase fluctuations are between 30 and 40 deg. Mean phase errors are about half of this.
- At millimeter wavelengths, the efficiencies are more like 0.78 and up to about 0.90 at the lowest frequencies; total residual phase fluctuations are between 20 and 30 deg. Mean phase errors are about half of this.

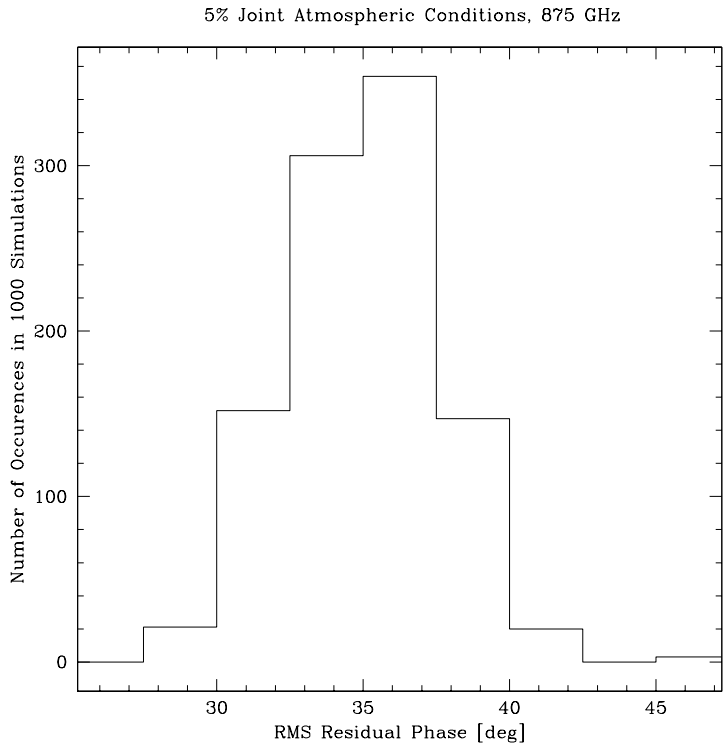

Figure 5: Histogram of the residual phase rms for the simulations reported on in Table 6 at 875 GHz.

- Quite surprisingly, dual-frequency fast switching is only marginally more effective than calibrating at the target frequency. Up to a target frequency of 345 GHz, calibrating at the target frequency is as efficient or more efficient than calibrating at 90 GHz, scaling the phases, and taking the extra time to perform the instrumental sequence.

So the reader can get a better feel for the sort of variation in the fast switching results due to the Monte Carlo simulations (which deals only with the randomness of the calibrator field), we show histograms of the 1000 results for the case of 875 GHz. Figure 5 shows the histogram of the total residual phase (87% of the simulations resulted in rms phases between 32.5 and 40 deg, and the median was 36 deg), and Figure 6 shows the histogram of the more narrowly peaked total efficiency for the fast switching process (87% of the simulations result in efficiencies between 0.65 and 0.75, with a median value of 0.69).

One surprising result that we can glean from this set of simulations is that fast switching will work pretty well even when calibrating at the target frequency. In fact, Calibrating at the target frequency should be almost as good as performing the calibration at 90 GHz and scaling to the target frequency, for target frequencies as high as 345 GHz. A marginal efficiency improvement is obtained at higher target frequencies – which, unfortunately, might *require* calibrating at the target frequency if there are problems with calculating the dispersive phase.

In retrospect, fast switching with the 90 GHz calibration frequency was designed for the MMA with 2000 m^2 collecting area. Now, with a much larger ALMA telescope and over

targetfreq	850	850	650	650	490	490	[GHz]
calfreq	90	850	90	650	90	490	[GHz]
el	60	60	60	60	60	60	[deg]
tau225	0.032	0.032	0.037	0.037	0.045	0.045	
rms300	0.79	0.79	1.155	1.155	1.615	1.615	[deg @ 11.2GHz]
all phase	31.53	36.70	33.09	37.86	33.77	38.78	[deg]
phase drift	9.073	6.940	8.974	6.630	9.208	6.626	[deg]
all eff0	0.749	0.691	0.734	0.677	0.727	0.666	
all eff1	0.872	0.845	0.868	0.845	0.865	0.845	
all eff2	0.859	0.814	0.846	0.803	0.840	0.795	
i.s. eff0	0.963	1	0.966	1	0.964	1	
i.s. eff1	0.972	1	0.975	1	0.975	1	
i.s. eff2	0.991	1	0.991	1	0.990	1	
t.s. eff0	0.777	0.691	0.760	0.677	0.754	0.666	
t.s. eff1	0.894	0.845	0.894	0.845	0.894	0.845	
t.s. eff2	0.867	0.814	0.854	0.803	0.849	0.795	
t.s. calflux	0.141	0.063	0.109	0.072	0.090	0.085	[Jy]
t.s. caldist	1.927	3.589	1.659	3.472	1.527	3.440	[deg]
t.s. tslew	1.724	2.360	1.592	2.295	1.529	2.273	[s]
t.s. tcal	0.447	4.746	0.381	3.622	0.318	3.436	[s]
t.s. tcycle	21.23	31.69	18.56	27.17	17.07	25.87	[s]
t.s. Ncycles	13.36	9.463	15.38	11.03	16.70	11.59	
t.s. ttarget	17.06	22.86	14.60	18.95	13.52	17.76	[s]
t.s. toverhead	4.184	8.941	3.851	7.774	3.595	7.599	[s]
t.s. phase	30.57	36.70	32.16	37.86	32.73	38.78	[deg]
t.s. atmophase	30.16	36.35	31.76	37.53	32.35	38.46	[deg]
t.s. gainerror	6.794	8.155	7.146	8.415	7.274	8.619	[deg]
i.s. calflux	1.136	-1	1.027	-1	1.124	-1	[Jy]
i.s. tarflux	0.326	-1	0.325	-1	0.402	-1	[Jy]
i.s. caldist	11.08	0	9.608	0	9.978	0	[deg]
i.s. tslew	5.546	0	4.938	0	5.085	0	[s]
i.s. tcal	4	0	4	0	4	0	[s]
i.s. tcycle	300	300	300	300	300	300	[s]
i.s. ttarget	283.7	300	285.5	300	285.1	300	[s]
i.s. toverhead	16.22	0	14.41	0	14.80	0	[s]
i.s. phase	7.658	0	7.602	0	7.941	0	[deg]
i.s. atmophase	5.264	0	5.886	0	6.204	0	[deg]
i.s. gainerror	5.569	0	4.810	0	4.957	0	[deg]
same cal	0.052	0	0.056	0	0.042	0	

Table 3: Median fast switching results for 850, 650, and 490 GHz, giving the best conditions to the high frequencies. (Since the median values of each distribution are reported, times or phase errors might not add up exactly as expected. Also, phase errors are for one baseline.) Note that the second (fourth, sixth) columns are for the same target frequencies, but performing fast switching calibration at the target frequencies instead of 90 GHz. "t.s." quantities are for an individual *target sequence*, "i.s." quantities are for the *instrumental sequence*, and "all" quantities refer to products of "t.s" and "i.s." quantities.

targetfreq	345	345	230	230	190	190	[GHz]
calfreq	90	345	90	230	90	190	[GHz]
el	60	60	60	60	60	60	[deg]
tau225	0.045	0.045	0.056	0.056	0.06	0.06	
rms300	1.84	1.84	2.175	2.175	3.21	3.21	[deg @ 11.2GHz]
all phase	28.90	30.03	24.68	25.05	27.52	28.06	[deg]
phase drift	7.055	4.852	5.919	4.281	6.582	4.385	[deg]
all eff0	0.788	0.782	0.834	0.840	0.807	0.807	
all eff1	0.897	0.894	0.916	0.925	0.906	0.912	
all eff2	0.880	0.871	0.911	0.908	0.891	0.886	
i.s. eff0	0.979	1	0.983	1	0.982	1	
i.s. eff1	0.985	1	0.986	1	0.986	1	
i.s. eff2	0.995	1	0.997	1	0.995	1	
t.s. eff0	0.805	0.782	0.849	0.840	0.821	0.807	
t.s. eff1	0.912	0.894	0.930	0.925	0.919	0.912	
t.s. eff2	0.884	0.871	0.913	0.908	0.894	0.886	
t.s. calflux	0.079	0.061	0.071	0.050	0.057	0.053	[Jy]
t.s. caldist	1.414	2.193	1.327	1.666	1.155	1.586	[deg]
t.s. tslew	1.487	1.825	1.449	1.588	1.371	1.552	[s]
t.s. tcal	0.283	0.538	0.216	0.327	0.177	0.325	[s]
t.s. tcycle	20.15	23.13	24.13	25.88	19.79	21.65	[s]
t.s. Ncycles	14.45	12.96	12.09	11.59	14.75	13.85	
t.s. ttarget	16.70	18.65	20.82	22.06	16.67	17.88	[s]
t.s. toverhead	3.441	4.499	3.282	3.779	3.112	3.693	[s]
t.s. phase	28.32	30.03	24.33	25.05	27.03	28.06	[deg]
t.s. atmophase	27.87	29.61	23.81	24.54	26.56	27.61	[deg]
t.s. gainerror	6.294	6.674	5.407	5.567	6.007	6.236	[deg]
i.s. calflux	0.338	-1	0.219	-1	0.197	-1	[Jy]
i.s. tarflux	0.130	-1	0.106	-1	0.110	-1	[Jy]
i.s. caldist	3.782	0	2.864	0	2.603	0	[deg]
i.s. tslew	2.395	0	2.093	0	2.008	0	[s]
i.s. tcal	4	0	4	0	4	0	[s]
i.s. tcycle	300	300	300	300	300	300	[s]
i.s. ttarget	291.2	300	291.8	300	291.9	300	[s]
i.s. toverhead	8.790	0	8.186	0	8.017	0	[s]
i.s. phase	5.566	0	4.298	0	5.154	0	[deg]
i.s. atmophase	4.977	0	3.922	0	4.781	0	[deg]
i.s. gainerror	2.492	0	1.757	0	1.922	0	[deg]
same cal	0.217	0	0.307	0	0.291	0	

Table 4: Median fast switching results for 345, 230, and 190 GHz, giving the best conditions to the high frequencies. Note that the second (fourth, sixth) columns are for the same target frequencies, but performing fast switching calibration at the target frequencies instead of 90 GHz. "t.s." quantities are for an individual *target sequence*, "i.s." quantities are for the *instrumental sequence*, and "all" quantities refer to products of "t.s" and "i.s." quantities.

targetfreq	145	145	90	70	35	[GHz]
calfreq	90	145	90	70	35	[GHz]
el	60	60	60	60	60	[deg]
tau225	0.089	0.089	0.129	0.129	0.22	
rms300	2.955	2.955	3.635	5.44	6.71	[deg @ 11.2GHz]
all phase	22.28	22.27	18.66	20.46	15.38	[deg]
phase drift	5.312	3.937	3.711	3.784	3.610	[deg]
all eff0	0.860	0.870	0.906	0.889	0.934	
all eff1	0.928	0.939	0.955	0.948	0.969	
all eff2	0.927	0.927	0.948	0.938	0.964	
i.s. eff0	0.984	1	1	1	1	
i.s. eff1	0.987	1	1	1	1	
i.s. eff2	0.998	1	1	1	1	
t.s. eff0	0.874	0.870	0.906	0.889	0.934	
t.s. eff1	0.939	0.939	0.955	0.948	0.969	
t.s. eff2	0.928	0.927	0.948	0.938	0.964	
t.s. calflux	0.056	0.048	0.042	0.059	0.033	[Jy]
t.s. caldist	1.153	1.329	1.029	1.117	0.753	[deg]
t.s. tslew	1.363	1.450	1.288	1.345	1.137	[s]
t.s. tcal	0.161	0.197	0.119	0.143	0.095	[s]
t.s. tcycle	26.81	27.60	32.86	29.41	41.84	[s]
t.s. Ncycles	10.89	10.86	9.127	10.19	7.169	
t.s. ttarget	23.74	24.32	29.97	26.40	39.30	[s]
t.s. toverhead	3.079	3.273	2.858	3.021	2.537	[s]
t.s. phase	21.98	22.27	18.66	20.46	15.38	[deg]
t.s. atmophase	21.41	21.71	17.98	19.84	14.55	[deg]
t.s. gainerror	5	5	5	5	5	[deg]
i.s. calflux	0.148	-1	-1	-1	-1	[Jy]
i.s. tarflux	0.099	-1	-1	-1	-1	[Jy]
i.s. caldist	2.246	0	0	0	0	[deg]
i.s. tslew	1.855	0	0	0	0	[s]
i.s. tcal	4	0	0	0	0	[s]
i.s. tcycle	300	300	300	300	300	[s]
i.s. ttarget	292.2	300	300	300	300	[s]
i.s. toverhead	7.711	0	0	0	0	[s]
i.s. phase	3.620	0	0	0	0	[deg]
i.s. atmophase	3.359	0	0	0	0	[deg]
i.s. gainerror	1.348	0	0	0	0	[deg]
same cal	0.377	0	0	0	0	

Table 5: Median fast switching results for 140, 90, 70, and 35 GHz, giving the best conditions to the high frequencies. Frequencies 90 GHz and lower use the target frequency for the calibration frequency. "t.s." quantities are for an individual *target sequence*, "i.s." quantities are for the *instrumental sequence*, and "all" quantities refer to products of "t.s" and "i.s." quantities.

targetfreq	875	937	[GHz]
calfreq	90	90	[GHz]
el	60	60	[deg]
tau225	0.029	0.029	
rms300	0.927	0.927	[deg @ 11.2GHz]
all phase	35.25	37.20	[deg]
phase drift	9.672	11.11	[deg]
all eff0	0.707	0.682	
all eff1	0.854	0.843	
all eff2	0.827	0.809	
i.s. eff0	0.962	0.953	
i.s. eff1	0.973	0.967	
i.s. eff2	0.989	0.985	
t.s. eff0	0.735	0.716	
t.s. eff1	0.881	0.866	
t.s. eff2	0.837	0.823	
t.s. calflux	0.128	0.128	[Jy]
t.s. caldist	1.797	1.798	[deg]
t.s. tslew	1.663	1.664	[s]
t.s. tcal	0.440	0.452	[s]
t.s. tcycle	17.93	16.96	[s]
t.s. Ncycles	15.85	16.56	
t.s. ttarget	13.70	12.89	[s]
t.s. toverhead	4.090	4.122	[s]
t.s. phase	34.15	35.74	[deg]
t.s. atmophase	33.78	35.38	[deg]
t.s. gainerror	7.590	7.942	[deg]
i.s. calflux	1.087	1.298	[Jy]
i.s. tarflux	0.312	0.362	[Jy]
i.s. caldist	10.61	12.78	[deg]
i.s. tslew	5.300	6.316	[s]
i.s. tcal	4	4	[s]
i.s. tcycle	300	300	[s]
i.s. ttarget	284.4	280.9	[s]
i.s. toverhead	15.59	19.01	[s]
i.s. phase	8.285	9.867	[deg]
i.s. atmophase	6.359	6.810	[deg]
i.s. gainerror	5.311	7.071	[deg]
same cal	0.052	0.035	

Table 6: Median fast switching results for 5th percentile conditions, which will be used to help set ALMA requirements.

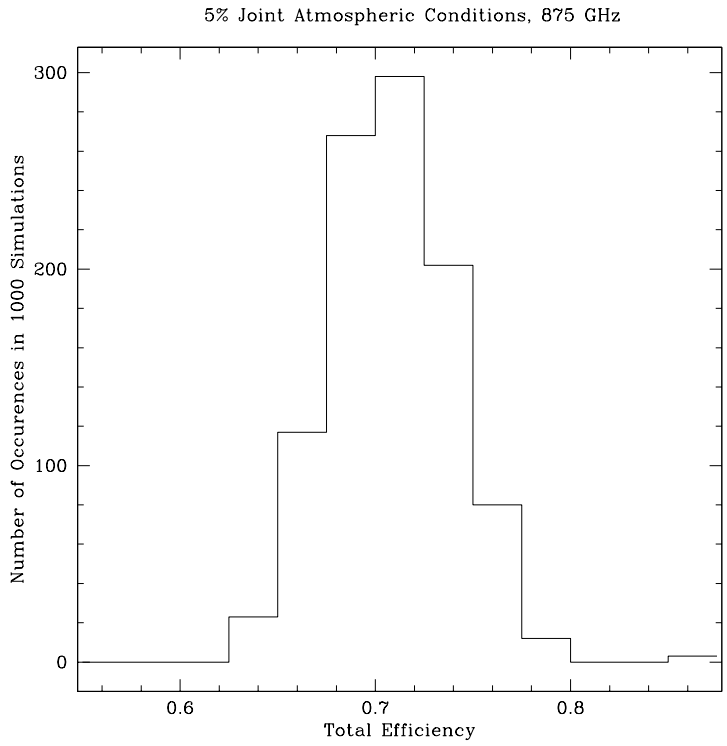

Figure 6: Histogram of the overall efficiency for the simulations reported on in Table 6 at 875 GHz.

7000 m^2 collecting area, the telescope is much more sensitive. The shortest part of the fast switching cycle is the time spent on the calibrator, so improving the telescope's sensitivity does little to improve fast switching with calibration observations at 90 GHz. However, it does a lot to improve fast switching with the calibration observations being performed at the target frequency.

7.1 Requirements on the Instrumental Stability

We suggest that the instrumental stability requirements can be derived from the results in Table 6, which have been run for opacity and phase conditions corresponding to the best 5% of Chajnantor atmospheric conditions. We consider two different sorts of requirements: rms instrumental delay jitter on timescales of a few tens of seconds (ie, the time scale of a single fast switching cycle), and the instrumental delay drift on time scales of about 300 s.

Our suggestion is that the instrumental phase fluctuations be equal to the atmospheric fluctuations in the 5^{th} percentile atmospheric conditions. There is some ambiguity about what the 5^{th} percentile conditions mean (we could take any pair of opacity and stability that lies on the 5^{th} percentile contours of the joint probability distribution of D'Addario and Holdaway, 2003), so we have taken those conditions which maximizes the array sensitivity at 875 and 937 GHz, considering both sensitivity losses due to phase fluctuations and opacity. This turns out to be close to 225 GHz opacity of 0.0296 and 11.2 GHz site testing interferometer phase of 0.927 deg for 875 GHz.

For the delay jitter, the relevant parameter here is the "all phase" number in the Tables above. To convert from phase ϕ, in degrees, to delay τ (sorry for the multiple use of Greek letters again)

$$\tau = \phi/360\ deg/\nu.$$

This gives 112 fs for the 875 GHz case and 110 fs for the 937 GHz case. Hence, we suggest that a baseline-based electronic and structural delay jitter specification for time scales up to a few tens of seconds of 111 fs is acceptable. Antenna-based would be 78 fs assuming that the phase fluctuations are independent among antennas.

Another number in the tables above is "phase drift". Part of this number is from the fairly small phase residuals from the instrumental sequence, which get frozen in over the 300 s full cycle; this is referred to as "i.s. phase" in the tables. There is also a contribution from the average phase jitter on each target sequence, though that averages down as $1/\sqrt{N_{cycles}}$. However, the phase jitter is calculated using γ_0, and for this determination, we need to use the smaller γ_1, which is appropriate for calculating the phase error. Hence, the phase drift over the entire 300 s calibration cycle can be calculated as

$$drift = \sqrt{\left(\left(\frac{\gamma_1}{\gamma_0} t.s.atmophase\right)^2 + t.s.gainnoise^2\right)/N_{cycles} + i.s.phase^2} \qquad (8)$$

Regarding the phase drifts, we find that the 5^{th} percentile visibility error due to residual atmospheric delay variation is 31 fs at 875 GHz and 33 fs at 937 GHz, so we'll average that to 32 fs. The instrumental error, is a combination of of drifts at the target frequency and the calibration frequency, should be made smaller than this. A part of the drifts will be common to both calibration and target bands (ie, antenna deformations or temperature-induced delay changes), and they will not contribute to the scaled phase difference, except to the extent that

the atmosphere at the target frequency is dispersive and a factor other than ν_{target}/ν_{cal} is used to scale the calibrator phase to the target frequency. Because the determination of the fraction of the delay drift which will be common to the two frequency bands is complicated and outside the scope of this work, we will not make a suggested delay drift specification, but rather assert that the drift in delay for the scaled frequency difference $\hat{\Phi}_i$ be 32 fs or better.

7.2 Impact of Instrumental Fluctuations

While the instrumental phase fluctuations of 111 fs will dominate the phase stability during only only the best 5% of observing conditions, these fluctuations will impact all observations, though low frequency observations are affected only marginally. Figure 7 shows how the instrumental fluctuations would degrade observations through additional decorrelation across the ten ALMA bands, parsing up the atmospheric conditions the way we have in the previous section. This figure is a bit bumpy because of odd variations in both the band sensitivity and the atmospheric conditions that are left for each lower frequency band. We define the integrated fractional sensitivity loss to be due to additional decorrelation by the instrumental phase errors:

$$\sum_{i}^{N_\nu} f_i(1 - e^{-(2\pi\tau\nu_i)^2/2}),$$

where the sum is over the frequency bands, f_i is the normalized fraction of time we observe in each band (ie, not counting time which is too bad to observe at any frequency), and τ is the instrumental delay specification (ie, 111 fs). This sum ends up being 0.037, so the total efficiency loss of ALMA due to this instrumental fluctuation specification, integrated over all bands, is under 4%. This is not an overly large burden, though the highest frequencies will carry most of that burden.

8 References

D'Addario, L., 2003, "Phase Calibration With Fast Switching: Implications for Instrumental Phase Stability", LAMA Memo 802.
D'Addario, L., and M.A. Holdaway, 2003, "Joint Distribution of Atmospheric Transparency and Phase Fluctuations at Chajnantor", LAMA Memo 801.

Butler, Bryan, 2003, "Distance to Possible Calibration Sources as a Function of Frequency for ALMA", ALMA Memo 478.

Condon, 1984, "Cosmological Evolution of Radio Sources", ApJ, 287, 461.

Delgado, Guillermo *et al.*, 2001, "Phase Cross-Correction of a 11.2 GHz Interferometer and 183 GHz Water Line Radiometers at Chajnantor", ALMA Memo 361.

Delgado, Guillermo *et al.*, 2003, "Some Error Sources For The PWV And Path Delay Estimated From 183 GHZ Radiometric Measurements At Chajnantor", ALMA Memo 451.

Feigelson, E.D., and Nelson, P.I., 1985, ApJ, 293, 192.

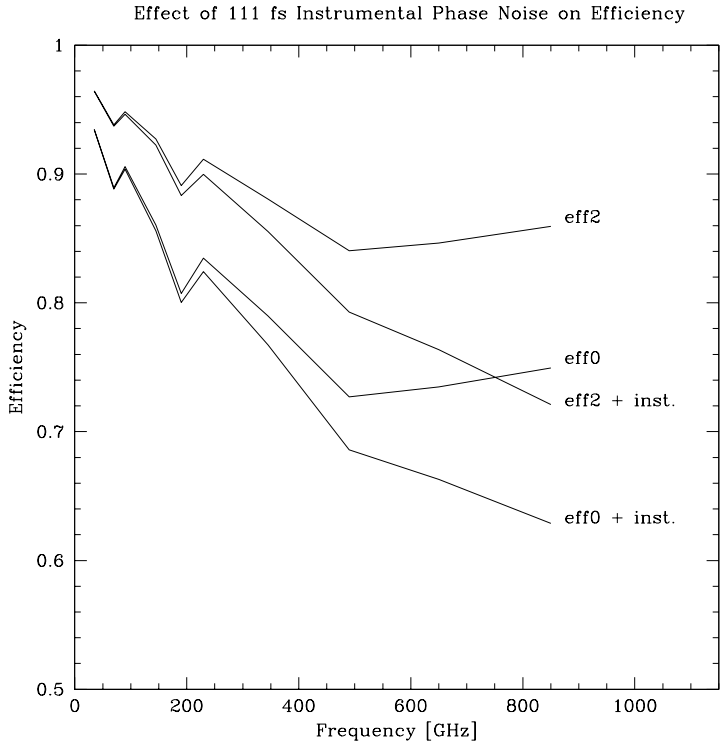

Figure 7: The affect of 111 fs instrumental delay jitter on the efficiency due to decorrelation only (eff2) and the total efficiency (eff0). The values of eff2 and eff0 are taken straight from Tables 3-5 and show the effect of the residual atmosphere and the inefficiencies of the calibration process, but no instrumental delay errors. The curves labeled "+ inst" indicate how the efficiencies are degraded when adding the 111 fs delay jitter.

Hills, R., and H. Gibson, 2001, "Design and Development of 183 GHz Water Vapour Radiometers", ALMA Memo 352.

Holdaway, M.A., F.N. Owen, and M.P. Rupen, 1994, " Source Counts at 90 GHz", ALMA Memo 123.

Holdaway, M.A., Simon J.E. Radford, F.N. Owen, and Scott M. Foster, 1995. " Data Processing for Site Test Interferometers", ALMA Memo 129.

Holdaway, M.A., 1996, " Calibration of Sub-millimeter Observations with SiO Masers: Does the MMA Need Dual Band Capability?", ALMA Memo 148.

Holdaway, M.A., and Mangum, Jeff, 2001, "Relative Pointing Sensitivity at 30 and 90 GHz for the ALMA Test Interferometer", ALMA Memo 373.

Holdaway, M.A., 2001, "Fast Switching Phase Correction Revisited for 64 12 m Antennas", ALMA Memo 403.

Holdaway, M.A., and Pardo, J.R., 2001, "Atmospheric Dispersion and Fast Switching Phase Calibration", ALMA Memo 404.

Holdaway, M.A., 2003, "Effects of Atmospheric Emission Fluctuations and Gain Fluctuations on Continuum Total Power Observations with ALMA", *to appear as a LAMA Memo.*

Holdaway, M.A., 2003b, *unpublished simulations of decorrelation and its correction.*

Patnaik et al, 1993, MNRAS 261, 435.

Radford, S.J.E., G. Reiland, and B. Shillue, Site Test Interferometer, *PASP*, *108*, 441-445, 1996.

A Defining Terms

We define the following terms in reference to Figure 1. Most of these terms will appear in the simulation results section in Tables 3 through 6.

- **target sequence tcal** is the time integrating on the weaker target sequence calibrator.
- **target sequence tslew** is the time it takes to slew from the target source to the target sequence calibrator source, or twice the frequency change time if it is longer than the slew time.
- **target sequence ttarget** is the time spent on the target source at the target frequency in a single target sequence cycle.
- **target sequence toverhead** includes both target sequence tcal and 2 * tslew, there and back, between the target source and the target sequence calibrator source.

- **target sequence tcycle** is the target sequence ttarget plus the target sequence toverhead, the time for a single complete cycle.

- **target sequence duty cycle** is the target sequence time on source divided by the target sequence cycle time.

- **target sequence eff1** is the efficiency due only to time lost from the target source during one target sequence cycle, and is given by the square root of the duty cycle.

- **target sequence effective baseline** is defined as $vt/s + d$, where v is the atmospheric velocity and t is the cycle time, and d is the distance between lines of site to the source and the calibrator.

- **target sequence atmophase** σ_ϕ^a is the atmospheric component of the target sequence residual phase error at the target frequency, and is approximately equal to the phase structure function evaluated at the target sequence effective baseline.

- **target sequence gainerror** is the error made in the gain phases, at the target frequency, due to finite SNR on the target sequence calibrator.

- **target sequence phase** σ_ϕ is the total phase error, rms, made by the fast target sequence cycles, and is equal to the sum in quadrature of the atmophase and the gainerror.

- **target sequence eff2** is the efficiency of the calibration process due to the target sequence phase errors, and is just the coherence given by

  $$eff2 = e^{-\sigma_\phi^2/2},$$

  with σ_ϕ being the target sequence phase (due to atmosphere and gain errors) in radians of phase at the target frequency.

- **target sequence eff0** is the product of target sequence eff1 and eff2. As the target sequence overhead time is determined by antenna capabilities and our need for accurate phase solutions, lengthening the target sequence cycle time will increase eff1, but will result in larger residual phase errors and lower eff2. As the cycle time decreases, the opposite trends are in play. For very short cycle times, the overall target sequence efficiency eff0 is low as eff1 tends toward zero. For very long cycle times, eff0 is low as eff2 tends toward zero. In between, there is an optimal cycle time, which will depend upon the atmospheric phase fluctuations and all. ALMA should be programmed to dynamically determine the target sequence cycle time which optimizes the target sequence efficiency eff0.

- **target sequence calibrator flux and calibrator distance** are the flux of the calibrator at the cal frequency, and the angular distance from the target source to the fast switching calibrator.

- **instrumental sequence tcal** refers to the total time, in 1 s sub-integrations, spent on the brighter instrumental sequence calibrator .

- **instrumental sequence tslew** is the time spent slewing from the target sequence phase calibrator to the instrumental sequence calibrator source.

- **instrumental sequence ttarget** is the time spent performing target sequence cycles (rather than instrumental sequence calibration).
- **instrumental sequence toverhead** is the instrumental sequence tcal plus twice the instrumental sequence tslew.
- **instrumental sequence cycle time (major cycle time)** is the instrumental sequence ttarget plus the instrumental sequence toverhead and is defined to be 300 s, the supposed instrumental stability time scale, in this work.
- **instrumental sequence duty cycle** is the instrumental sequence time on source divided by the instrumental sequence cycle time.
- **instrumental sequence eff1** is the efficiency due only to time lost to the instrumental sequence sequence or toverhead, and is the square root of the instrumental sequence duty cycle.
- **scaled instrumental phase difference** Φ_i will be the instrumental phase at the target frequency minus the instrumental phase at the cal frequency scaled by the ratio of the frequencies:
$$\Phi_i = \phi_i(\nu_{tar}) - \phi_i(\nu_{cal}) \cdot \nu_{tar}/\nu_{cal}.$$
- **instrumental sequence atmophase** is the atmospheric contribution corrupting the scaled instrumental phase difference, and ends up being the root structure function evaluated at about 2 s.
- **instrumental sequence gainerror** is the error in the scaled instrumental phase difference Φ_i due to the influence of thermal noise on the gain phase determinations.
- **instrumental sequence phase** is the overall phase error in the determination of the scaled instrumental phase difference Φ_i, and is equal to the sum in quadrature of the instrumental sequence gain error and the instrumental sequence atmophase.
- **instrumental sequence eff2** is the efficiency of the instrumental sequence calibration process due to instrumental sequence phase errors, and is equal to the coherence due to the instrumental sequence phase errors.
- **instrumental sequence eff0** is the product of instrumental sequence eff1 and eff2, and is a measure of the overall efficiency of the instrumental sequence calibration.
- **instrumental sequence cal flux** is the flux of the instrumental sequence calibrator at the calibration frequency.
- **instrumental sequence target flux** is the flux of the instrumental sequence calibrator at the target frequency.
- **all eff1** is the efficiency due to time lost from the target source by both target sequence and instrumental sequence calibration.
- **all eff2** is the efficiency due to residual phase errors, both atmospheric and noise-like, from both target sequence and instrumental sequence calibration.

- **all eff0** is the overall efficiency of the target sequence and instrumental sequence calibration processes, and is equal to all eff1 times all eff2. We seek a target sequence and instrumental sequence strategy which optimize the quantity all eff0.